JOURNAL OF GEOPHYSICAL RESEARCH: OCEANS, VOL. 118, 1459–1472, doi:10.1002/jgrc.20124, 2013

Water and suspended sediment division at a stratified tidal junction

F. A. Buschman,[1,2] M. van der Vegt,[1] A. J. F. Hoitink,[1,3] and P. Hoekstra[1]

Received 1 June 2012; revised 5 February 2013; accepted 7 February 2013; published 25 March 2013.

[1] Tidal junctions play a crucial role in the transport of water, salt, and sediment through a delta distributary network. Water, salt and sediment are exchanged at tidal junctions, thereby influencing the transports in the connecting branches and the overall dynamics of the system. This paper presents observations of water, salt and sediment transports in three channels that connect at a stratified tidal junction. Flow variation in one channel was found to lag behind flow variation in a connected channel by more than 1 h, which is largely attributed to channel length differences from the junction to the sea. The water columns in the three channels were periodically stratified during spring tide, whereas the salinity structure represented a salt wedge during neap tide. Salinity differences between the three channels were substantial. The channels contain water bodies of different salinity and act largely independently. Flow velocities in the upper and lower layers differed substantially. Flow in the lower layer was generally in the direction of acceleration produced by the baroclinic pressure gradient. Interestingly, baroclinic pressure gradients were sometimes directed landward, indicating the presence of saltier water at the land side of the estuary. In sharp channel bends close to the junction, secondary flow was strongest at the highest axial flow velocity during spring tide. In one channel bend, these circulations steered the suspended sediment toward the inner bend, which affected the suspended sediment division.

Citation: Buschman, F. A., M. van der Vegt, A. J. F. Hoitink, and P. Hoekstra (2013), Water and suspended sediment division at a stratified tidal junction, *J. Geophys. Res. Oceans*, *118*, 1459–1472, doi:10.1002/jgrc.20124.

1. Introduction

[2] The division of water and suspended sediment at junctions is important for the transport of water, sediment, and solutes such as salt through tidal channel networks. The division of suspended sediment at a tidal junction impacts on the morphological development of the tidal network, which is relevant for navigation and engineering works. Regarding the ecology of tidal networks, tidal junctions control the distribution of contaminants including dissolved pollutants, which impact the aquatic environments [*Turner and Millward*, 2002]. Hence, tidal junctions play a key role in the hydrodynamic, morphological, and ecological functioning of tidal networks.

[3] The bulk of the scientific work on flow and sediment transport in estuaries is focused on single channels. The dynamics of estuaries that consist of multiple connecting channels have received little attention. The hydrodynamics of estuarine channel networks are generally more complex than in a single channel. The flow dynamics in the various channels interact, and these interactions may vary with the tides. Tides propagate from the sea through the sea-connected branches. At tidal junctions, the tidal energy is distributed over the connecting channels. Differences in geometry between the connecting channels result in strong differences in amplitude and phase of the tidal flow at the junction [*Seim et al.*, 2006; *Warner et al.*, 2002]. Channel length and width variations control the propagation and reflection of tidal wave energy, which determines the character of the tide. Although observations from channels around tidal junctions have previously been reported, the physical mechanisms behind these observations were often left unexplored.

[4] This contribution aims at improving our understanding of the dominant processes at tidal junctions by describing and analyzing field observations obtained at a tidal junction in an estuarine channel network located in Kalimantan, Indonesia. The observations were carried out at the tidal junction located north of station Tambak in the estuarine channel network (Figure 1). This system was chosen because of the high ecological value of the area and the rapid economic development that poses severe threats to the ecosystem health. The tidal network under study connects the sea with the Berau River, which is located in between Gunung Tabur and the first junction where the river splits

[1]Institute for Marine and Atmospheric Research Utrecht (IMAU), Department of Physical Geography, Faculty of Geosciences, Utrecht University, Utrecht, The Netherlands.

[2]Now at: Rijkswaterstaat Centre for Water Management, Ministry of Infrastructure and the Environment, Utrecht, The Netherlands.

[3]Hydrology and Quantitative Water Management Group, Department of Environmental Sciences, Wageningen University, Wageningen, The Netherlands.

Corresponding author: F. A. Buschman, Water Management Division, Rijkswaterstaat, PO Box 17, Lelystad, Utrecht, 8200 AA, The Netherlands. (frans.buschman@gmail.com)

2169-9275/13/10.1002/jgrc.20124

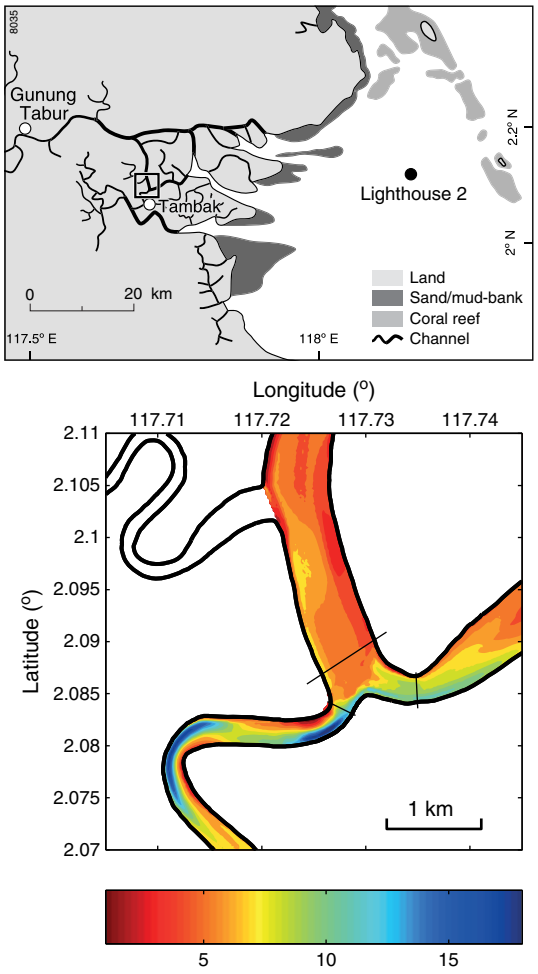

Figure 1. Topographical map of the Berau region with the tidal junction under study indicated is shown in the top panel. The bottom panel shows the bathymetry around the tidal junction, showing depths in meters below mean sea level, and shows a grid across each of the channels where observations are projected on.

in the estuarine channel network. In the adjacent sea, large coral reef assemblages are present. Increasing suspended sediment loads due to land use changes may be transported to these reef complexes by the freshwater plumes that spread out over the inner shelf (A. Tarya et al., Tidal control over river plume spreading in a near-equatorial region, submitted to *Journal of Geophysical Research*), which will pose an increasing threat to the coral reef health [*Buschman et al.*, 2011].

[5] In a modeling study, *Buschman et al.* [2010] showed how the subtidal water division at a channel junction can respond to properties of channel geometry, including length, width, and depth, and bottom roughness. They found that tides enhance the inequality in the division of river water in the case of geometric differences between the channels, while it reduces the inequality in the case of bottom roughness differences between the channels. Also, local topography and bathymetry at a tidal junction affect water division [*Kim and Voulgaris*, 2005; *Sassi et al.*, 2011]. *Sassi et al.* [2011] recently demonstrated that differences in water level setup caused by nonlinear interaction between river, and tidal flow in adjacent distributaries asserts an additional control over the division of river water in a channel network. The mechanism they termed differential water level setup favors the allocation of river water to relatively small distributaries. The present contribution continues this line of research by focusing on processes of sediment and salt division at a tidal junction, which connects a tidal meander to a river distributary.

[6] In river networks, the division of sediment transported as bed load at bifurcations has received ample attention in the literature, which was reviewed by *Kleinhans et al.* [2013]. Processes controlling the division of suspended sediment have been studied in less detail, while in downstream parts of rivers and estuaries, suspended sediment transport often becomes dominant over bed load transport [*Dyer*, 1986; *Prandle*, 2004]. It is often simply assumed that suspended sediment divides and combines approximately as the discharge [*Fassnacht*, 2000]. This implies that suspended sediment is transported as a passive tracer and is distributed uniformly over the cross-section. At bifurcations and confluences, this assumption is doubtful, because deposition and resuspension of sediment are substantial [*Fassnacht*, 1997, 2000; *Warner et al*., 2003]. The tidal motion and baroclinic pressure gradients at tidal junctions will influence the net division of water and suspended sediment in several ways.

[7] In single-channel, partially mixed estuaries, the interaction of along-channel and cross-channel density gradients and tidal flow results in a net vertical residual circulation that tends to intensify at neap tide, when turbulent mixing is reduced [e.g., *Jay and Flinchem*, 1990; *Stacey et al*., 2001]. Under these circumstances, the net flow near the bottom is landward, whereas near the surface it is directed seaward. This estuarine circulation will affect the transport of sediment at the junction. Observations have shown that near-tidal junctions, salinity gradients may be locally reversed, implying that salinity increases in the landward direction. This results in a reversed estuarine circulation [*Warner et al.*, 2002]. Further away from the junction, the salinity gradient resumes its "classical" pattern. Hence, in the region of a tidal junction, freshwater and sediment may be trapped. Whereas *Warner et al.* [2002] observed the reversed estuarine circulation at the junction of two straights in San Francisco Bay, herein we show that the same process can occur in a shallow estuarine channel network.

[8] Cross-channel flows strongly impact the distribution of sediment over the cross-section in estuaries [*Huijts et al.*, 2006]. In the case of curvature-induced secondary flow, high-concentration sediment suspensions are typically steered toward the inner bend. Secondary flows are also generated by cross-channel density gradients, advective processes and earth rotation effects. In turn, secondary flows substantially affect the stratification dynamics when the axial flow velocities and turbulent mixing are sufficiently large to overturn the stratified water column [*Seim and Gregg*, 1997; *Lacy and Monismith*, 2001; *Chant*, 2002; *Lerczak and Geyer*, 2004]. This contribution shows that secondary flows may be pronounced in one of the three connecting channels, although the stratification in that channel is relatively strong. The secondary flows in that channel may be enhanced by baroclinic pressure gradients, whereas in the other channels, baroclinic pressure gradients suppress the curvature-induced circulation.

[9] The main objective of this paper is to show how barotropic and baroclinic processes affect the transport of water, salt, and sediment at a tidal junction. The remainder of this paper is constructed as follows. The next section describes the *field site*. Subsequently, the *data acquisition and processing* are detailed, including a discussion on the derivation of the transports from measured data. The *results* show the water level variation, salinity profiles, flow velocity patterns, suspended sediment concentrations, and the transport of water, salt, and sediment at the junction. The *discussion* describes four key aspects that affect the intratidal division functions. The paper ends with *conclusions*.

2. Field Site

[10] The Berau estuarine channel network constitutes the delta of the Berau River, located along the east coast of Kalimantan, Indonesia (top panel of Figure 1). The tidal network consists of three large west-east oriented branches, which are interlinked. The northern branch is shallowest, with a typical mean depth of 5 m. The middle branch is about 7 m deep and the southern branch is deepest, having a mean depth around 10 m. Deep trenches in the channels occur, especially in sharp bends and close to the tidal junctions. The bottom panel of Figure 1 shows the bed levels around the tidal junction under study. The bed levels shown were obtained by navigating transects across the channels, with an interspacing of about 1 km, with an echo sounder and a GPS. The raw data were corrected for water surface level variation using nearby level gauges and interpolated along the channel. Especially the channel west of the tidal junction subject to study, which connects the middle and southern branches, has sharp bends with deep trenches in the outer parts of the bends. The trench closest to the tidal junction has a maximum depth of 18 m.

[11] The system is dominantly forced by river discharge and tides. Based on an observation period of 6 months in 2007, *Buschman et al.* [2009] showed that the river discharge averaged 605 m^3s^{-1} and that it may vary relatively rapidly. Within 3 days, the river discharge can increase from below average to the maximum observed river discharge, which amounted to about 1400 m^3s^{-1}. This peak river discharge was about half of the peak discharge at spring tide measured at Gunung Tabur (top panel of Figure 1), which is located in the tidal river. During spring tide, the peak ebb and peak flood discharge were similar, whereas during neap tides, the peak ebb was larger than peak flood discharge. Since winds were maximally moderate during the observation period, the wind forcing was assumed to be of secondary importance.

[12] Tides propagate into the Berau tidal network at the three main branches. The tidal range is about 1 m at neap tide and about 2.5 m at spring tide and has a pronounced diurnal inequality. Table 1 shows the results of an harmonic analysis of surface elevation at Lighthouse 2, a station located on the inner shelf close to the outlet of the three main branches (see top panel of Figure 1). The diurnal constituents K_1 and O_1 both have an amplitude of about 23% of the M_2 amplitude. The tidal range largely remains unchanged going landward in the tidal river, at least up to Gunung Tabur [*Buschman et al.*, 2009].

Table 1. Harmonic Analysis of the Water Surface Elevation at Lighthouse 2 for Eight Tidal Constituents [*Tarya et al.*, 2010]

Tidal Constituent	Amplitude (cm)	Phase (°)
M_2	70	350.57
S_2	42	220.98
N_2	10	295.26
K_2	11	243.38
K_1	17	155.61
O_1	16	12.63
P_1	7	303.79
Q_1	3	10.86

3. Data Acquisition and Processing

3.1. Flow Velocity

[13] A 1.2 MHz broadband RD Instruments acoustic Doppler current profiler (ADCP) was mounted at approximately 0.23 m below the water surface from the side of a wooden fishing boat. The ADCP measured continuously in mode 1 and was connected to the GPS. The range to the first ADCP cell center was 1.09 m and the cell size was 0.30 m. Flow velocities across and along the channel were obtained by crossing the three channel transects each half an hour, during a 12.5 h period at spring tide and at neap tide. The measured flow velocities were projected on a cross-channel grid (bottom panel of Figure 1) with a horizontal spacing of 2.0 m and 101 sigma layers in the vertical. The instantaneous flow velocities were smoothed using a moving average over 42 m in the horizontal and five sigma layers in the vertical direction.

[14] Flow velocities could not be measured near the surface and near the bed. Axial flow velocities in these regions were determined by extrapolation, roughly following the methods of *Muste et al.* [2004]. All axial velocity profiles were extrapolated to the bottom adopting a one-sixth power law profile. In most cases, this power law was also used for the extrapolation to the water surface. When the measured axial flow velocity profile changed sign below 2.5 m from the water surface, the flow velocity profile was linearly extrapolated toward the surface. In the remaining few cases in which flow velocity changed sign close to the water surface, the flow velocity in the highest grid cell was assigned to the entire upper layer. The across channel velocity profiles were not extrapolated.

3.2. Density Gradients

[15] Vertical salinity and temperature profiles were obtained each hour, using a Seabird conductivity-temperature-depth (CTD) device at a fixed and relatively deep location in each channel. Only data from the upcasts were used, since it is easier to manually lift the CTD at a steady pace than to lower it. Salinity and temperature data were projected on the same grid as the velocity data. Temperature and salinity are assumed uniform over width. Density was derived from temperature and salinity, using the equation of state.

[16] Using the density profiles, the potential energy anomaly ϕ was calculated. This is a measure for the degree of stratification and quantifies the energy that is needed to mix the water column [*Simpson*, 1981],

$$\phi = 1/d \int_{-h}^{\zeta} gz(\bar{\rho} - \rho(z))\mathrm{d}z. \quad (1)$$

Here, g is the gravitational acceleration, $d = h + \zeta$ is the total water depth, $z = -h$ is the position of the bed, ρ is the density, and $\bar{\rho}$ is the depth-averaged density. Water level ζ was measured at Tambak station, which is located at 5 km from the tidal junction in the western channel (top panel of Figure 1). The rate of change of ϕ due to tidal current mixing was estimated according to

$$\frac{\partial \phi}{\partial t}_{\text{mix}} = -\Gamma c_d \rho_0 \frac{|\bar{u}^3|}{d}, \tag{2}$$

where Γ is mixing efficiency, c_d is the drag coefficient, and ρ_0 is the density of sea water. To estimate the rate of change of ϕ by mixing, we attribute $\Gamma = 0.04$ and assume $c_d = 0.0025$ [*Burchard and Hofmeister*, 2008; *Hoitink et al.*, 2011].

[17] Horizontal density differences between the channels result in baroclinic pressure gradients. The baroclinic pressure gradients between the three channels were determined at 5 m below the mean datum, which coincides with the bed of the shallowest channel:

$$\frac{\Delta p_c}{\Delta s} = g \int_{-5}^{\zeta} \frac{\rho_i(z) - \rho_j(z)}{\Delta s_{ij}} \mathrm{d}z, \tag{3}$$

where $\rho_i(z)$ and $\rho_j(z)$ are the density profiles in the northern, eastern, or southern channel and Δs_{ij} is the horizontal distance between two density profiles.

3.3. Suspended Sediment Concentration

[18] An optical backscatter sensor (OBS) was attached to the CTD device. The turbidity measurements were related to suspended sediment concentration (c) by calibration with in situ water samples, as described in detail for the Berau River in *Buschman et al.* [2011]. For the tidal junction measurements, in total 72 water samples were used for the calibration. Calibration with the corresponding turbidity measurements resulted in almost the same relation as for data obtained at other locations in the delta [*Buschman et al.*, 2011]. The latter relation was also used in this study.

[19] The spatial variation of the suspended sediment concentration in the cross-section was determined by using the OBS-derived estimates of suspended sediment concentration to calibrate the ADCP backscatter signal. Details of the methods that were used can be found in *Deines* [1999], *Downing et al.* [1995], *Thorne and Hanes* [2002], *Gartner* [2004], and in *Hoitink and Hoekstra* [2005]. The suspended sediment concentration obtained from the ADCP echo intensity covered most of the cross-section, but in the top 2.0 m of the water column and near the bed, no reliable echo intensities were obtained. To fill the gaps, the highest optically observed suspended sediment concentration was assigned to the full width of the particular cross-section. In between this optically derived value at 0.5 m below the water surface and the acoustical observations at 2.0 m from the water surface, suspended sediment concentration was linearly interpolated. In the layers near the bottom and surface where neither acoustical nor optical observations were made, the suspended sediment concentration was obtained via a linear extrapolation.

3.4. Transports

[20] Transports of water, freshwater, and sediment in the three channels were calculated using similar methods as described in *Muste et al.* [2004]. Their method was originally developed to calculate discharges in riverine channels, and the error in the obtained discharge is estimated to be 2.5% of the obtained value. Based on their method, the transport of any constituent consists of a part in the central section of the channel and of parts in the regions near the shores that could not be measured.

[21] The transport of X in the central section of the channel was calculated by

$$T_{X,\text{mid}} = \int_{n_s}^{n_e} \int_{-h}^{\zeta} u(z,n) X(z,n) \mathrm{d}z \mathrm{d}n, \tag{4}$$

where n_s is where observations in the cross-section started and n_e where a transect ended. For the discharge (total water transport Q), X equals 1. To calculate the freshwater transport (Q_f), X was set to the fraction of freshwater f:

$$f = \frac{Sa_{\text{sea}} - Sa}{Sa_{\text{sea}}}, \tag{5}$$

where Sa represents the measured salinity and Sa_{sea} is the maximal salinity at sea, which was 35 practical salinity unit (psu). For the suspended sediment transport (S), X is the suspended sediment concentration.

[22] The contributions of the regions near the shores to the discharge were estimated as the product of the unmeasured wetted cross-section and one third of the depth-mean velocity measurement closest to the bank. The contributions of the regions near the sides of the channel to Q_f and S were determined by multiplying the water transport near the banks with the depth-mean value of the measured freshwater fraction and the suspended sediment concentration closest to the side, respectively.

4. Results

4.1. Water Level and Discharge

[23] The observation periods started around high water on both days (top row of Figure 2). Due to the diurnal inequality, the high water level at the start of the spring tide survey was higher than the high water level at the end of the survey. The neap tide observations started at lower high water.

[24] The bottom row of Figure 2 shows the discharge during the observation periods. As a test for the accuracy of the discharge observations, the difference between the discharge in the northern and the sum of discharges in the western and eastern channels is presented. Averaged over the tidal periods, the absolute difference is small compared to the absolute discharges in the individual channels, suggesting that the discharge derivations can be considered accurate. Due to the diurnal inequality, subtidal transports could not be obtained accurately from the 13 h observations.

[25] The observations at spring tide started around the end of flood tide. The eastern channel was close to high water slack, while in the northern and western channels, still flood conditions occurred. The times of slack water differed substantially between the channels. High water slack occurred half an hour later in the northern channel and 1.5 h later in the western channel than in the eastern channel. The time

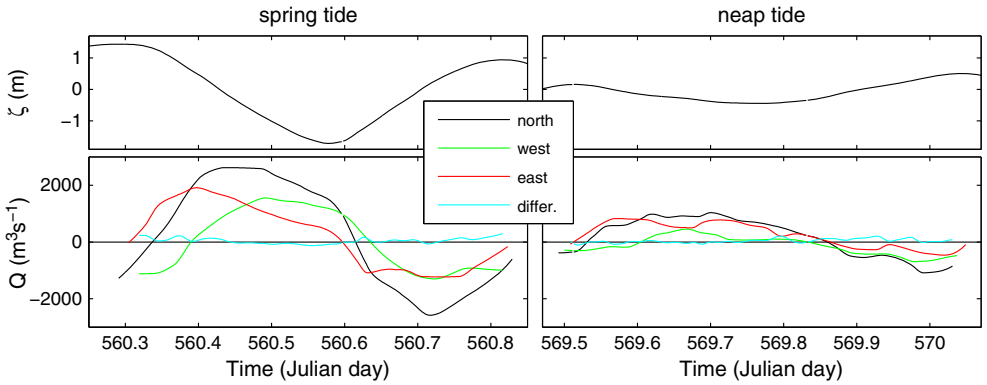

Figure 2. Measured water levels (top row) and discharges (bottom row) at the junction around spring tide (left column) and around neap tide (right column). Positive discharge indicates ebb flow, which is directed southward in the northern channel, westward in the western channel, and eastward in the eastern channel. The bottom panels also present the discharge in the northern channel minus the sum of discharges in the other two channels.

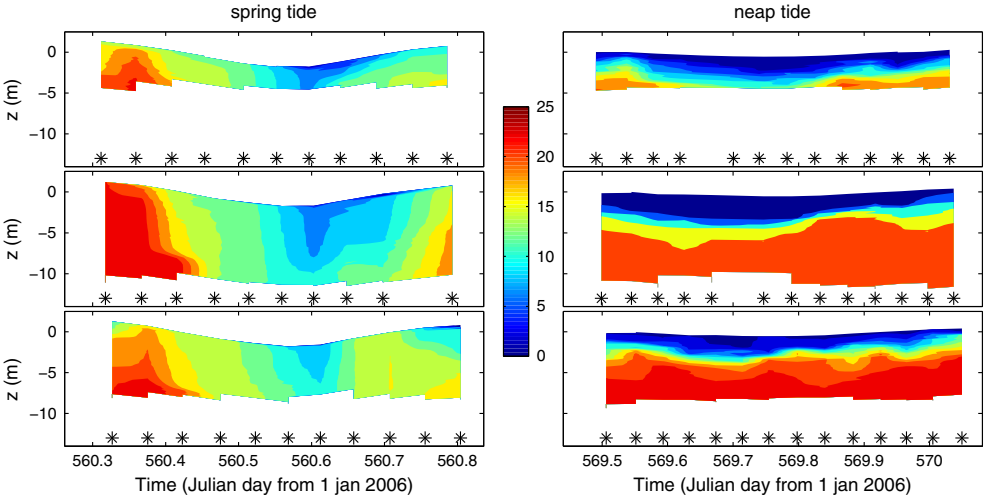

Figure 3. Salinity (psu) in the northern (top row), western (middle row), and eastern channel (bottom row) during spring tide and neap tide. Stars indicate moments when CTD profiles were taken.

differences of low water slack occurrence had the same sign, but were smaller. During neap tide, high water slack also occurred first in the eastern channel, then 20 min later in the northern channel, and 2 h later in the western channel. Low water slack at neap tide occurred first in the western channel, implying that the ebb tide duration was shortest in this channel.

4.2. Salinity Profiles

[26] The measured salinity profiles at the three channels near the junction are shown in Figure 3. The water columns were partially mixed during spring tide and highly stratified during neap tide. The average difference between top and bottom salinity was 21 psu during neap tide. The potential energy anomaly was higher than 100 J m^{-3} throughout the entire tidal cycle and showed little time variation (middle right panel of Figure 4). Furthermore, there are pronounced differences between the three channels, with the western channel having the highest value. During spring tide, ϕ showed more time variation in the three channels (middle of left column in Figure 4). The potential energy anomaly is lowest at peak ebb flow in the northern channel. The northern channel is shallowest and had the highest cross-section averaged flow velocities, which enhanced mixing. The bottom of left column in Figure 4 shows that the rate of change of ϕ due to mixing has indeed the largest magnitude in the northern channel. In all three channels, the highest degree of stratification occurred around high water slack. The peak in the western channel was most pronounced, which may be related to the flow phase differences.

[27] Based on the measured and gridded salinity profiles, we also determined the baroclinic pressure gradients between the three channels. These pressure gradients at the bed level of the shallowest channel are shown in the top row of Figure 4. The north to east (N-E) baroclinic pressure gradient $\Delta p_c/\Delta s$ was derived according to equation (3), where ρ_j is density in the eastern channel, ρ_i is density in

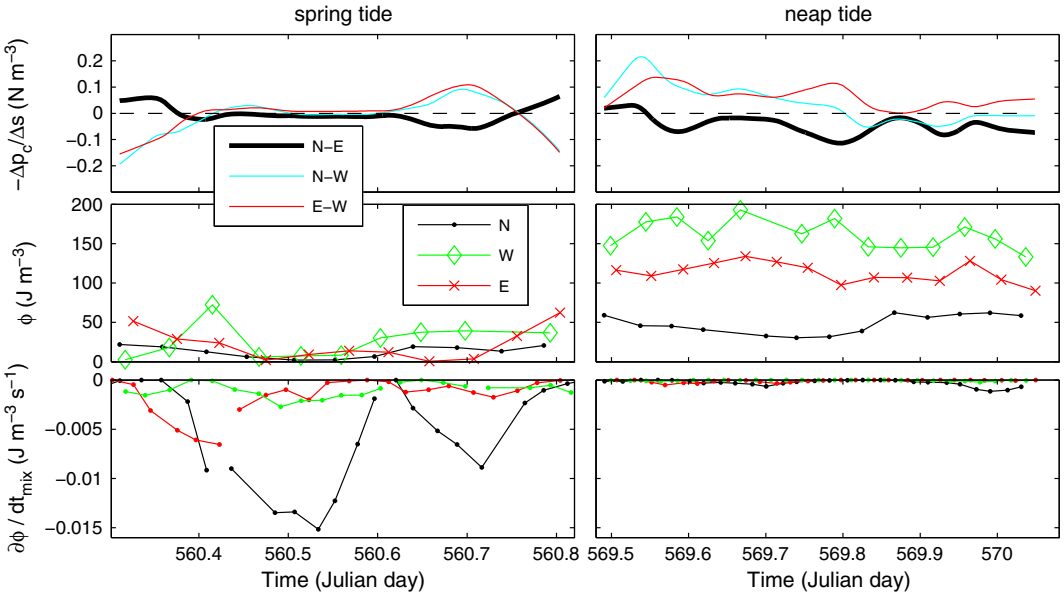

Figure 4. The baroclinic pressure gradient between the cast locations at the averaged bed level in the northern channel (top row), the potential energy anomaly at the three cast locations (middle row), and its time rate of change (bottom row).

the northern channel, and Δs is the distance between the cast locations in the northern and eastern channels. Similarly, the N-W (E-W) values of $\Delta p_c/\Delta s$ were determined by subtracting the baroclinic pressure in the northern (eastern) channel from that of the western (western) channel. A positive N-E gradient implies that the eastern channel has more saline water than the northern channel.

[28] During spring tide, absolute values of $\Delta p_c/\Delta s$ were small during the ebb phase and relatively large during the flood phase. At the beginning of the flood phase, a baroclinic pressure gradient was directed from the northern to the western channel. Hence, at that moment the northern channel featured a higher salinity than the western channel and the salinity gradient is opposite to what is generally observed in single channel estuaries. The eastern channel was more saline than the northern channel and can be considered as the source of the saline water in the northern channel. At the end of the flood phase, the baroclinic pressure gradients reversed again. During this period, the western channel was most saline, while the northern channel was more saline than the eastern channel. The baroclinic pressure gradient directed from the northern to the eastern channel was then again opposite to what may have been expected from the fact that the northern channel connects directly to the Berau River.

[29] During neap tide, a baroclinic pressure gradient was directed from the eastern channel to the western channel during the entire tidal cycle. Figure 3 shows that this direction of $\Delta p_c/\Delta s$ was caused by the relatively thick freshwater layer in the western channel. Between the northern and the eastern channels, $\Delta p_c/\Delta s$ was directed toward the northern channel, except for a short period around high water slack. Between the northern and western channels, $\Delta p_c/\Delta s$ was directed from the western to the northern channel during the flood phase, but reversed during the ebb phase.

4.3. Flow Velocities

[30] The flow velocity vectors were averaged over the top and bottom half of the water column. Figure 5 shows the flow velocities in these layers for six moments during the spring tide survey. The top of the left column corresponds to high water slack. At that moment, the western and northern channels still experienced flood flows, while the eastern channel already displayed ebb flow, which was concentrated in the lower layer. The flow direction and magnitude in the northern channel were highly variable. In the western channel, the persistent difference in flow direction between the top and lower layers reveals a strong influence of secondary flows. The next two panels (top row of middle and right columns) show flows at maximum ebb. Especially at t = 560.42, flow in the lower layer was predominantly from the northern to the eastern channel, while flow in the upper layer divided about equally over the western and eastern channels. In the curved western and eastern channels, cross-channel circulation may be present. The cross-channel flow in the western channel was likely caused by channel curvature, while in the eastern channel, it opposed the circulation that may potentially be induced by curvature.

[31] The bottom of the left panel in Figure 5 shows flow velocities during low water slack (t = 560.61). Flow velocities in the lower layer were larger than those in the upper layer. The eastern channel already displayed flood flows, while in the western channel, the ebb was still prevalent. Water from the eastern channel is transported both to the east side of the northern channel and to the western channel. In the western channel again strong secondary flows were present that may be caused by channel curvature. The bottom of the middle column shows the flow velocities at maximum flood (t = 560.71). The northern channel received water both from the western and from the eastern channel. The bottom flows in the northern channel showed to be more

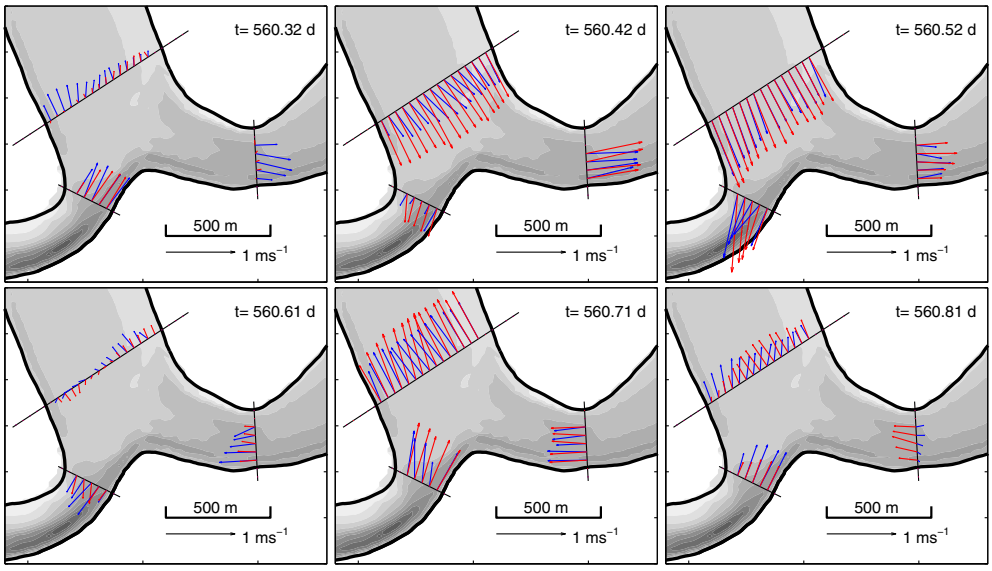

Figure 5. Depth-averaged flow velocities of the top (red vectors) and bottom (blue vectors) half of the water column at spring tide, plotted with 2.4 h time interval.

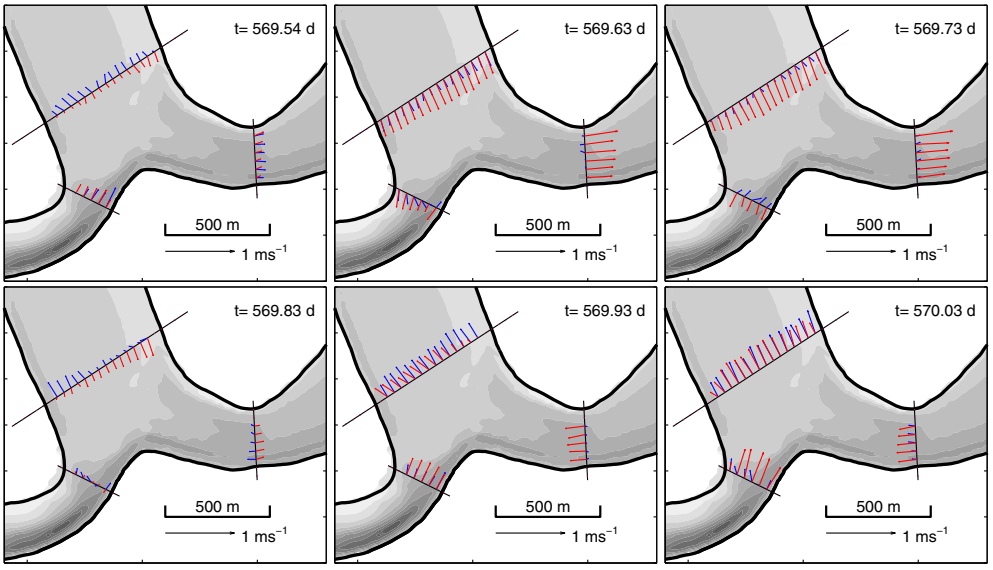

Figure 6. The same as Figure 5, but now for six moments during neap tide.

westerly directed, while the surface flow was more to the east. This pattern corresponds with the flow velocity patterns in the eastern and western channels, where also a clockwise change in flow direction between upper and lower layer can be observed. The bottom of the right column corresponds to a moment just before high water slack (t = 560.81). At that time, flow patterns were similar to the flow patterns described for the top of the left column.

[32] Figure 7 depicts the layer-averaged flow velocity patterns in the upper and lower layers at neap tide. Flow velocities were much smaller than during spring tide. Flows in the upper and lower layers were decoupled, due to strong stratification. In the eastern channel, flows mainly occurred in the upper layer, while near the bottom the water mass was almost stagnant. The top of the left column (t = 569.54 d) shows the flow velocities around high water slack. In the eastern channel, the flow direction had already reversed, while in the western channel, still flood flows occurred. In the northern channel, flows had reversed near the surface, but not near the bottom. This implies that the upper layer of the eastern channel received water from the northern and from the western channels, while near the bottom the western channel was exchanging water with the northern and eastern channels. The eastern channel may have been subject to a low intensity secondary circulation. The top of the middle column (t = 569.63 d) corresponds to about 1 h before maximum ebb. The lower layer of the eastern channel had small flows directed in the flood direction. The flows in the western channel indicate that a secondary circulation occurred, opposite to the sense of rotation in

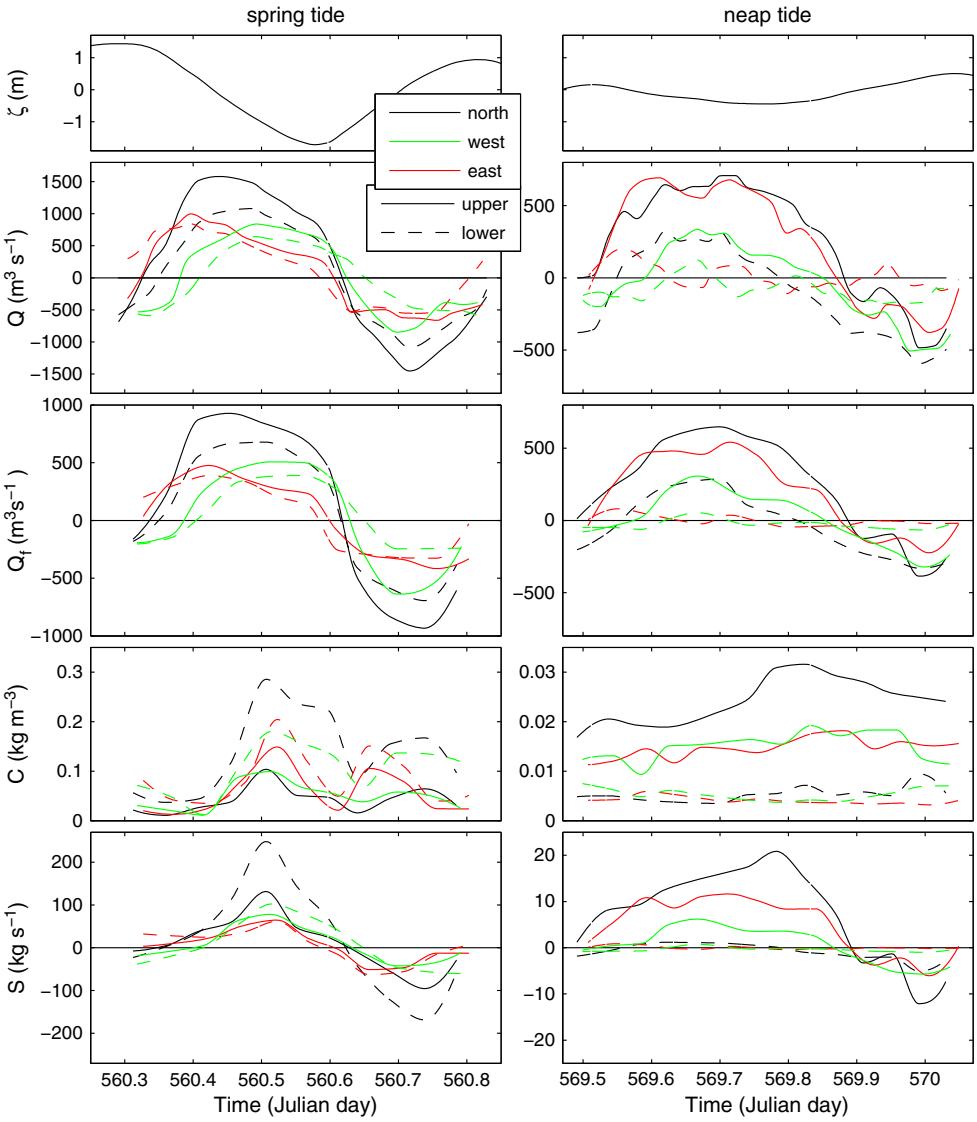

Figure 7. Water surface level (top row) and in the upper and lower layers: the total water transport (second row), the freshwater transport (third row), the cross-sectionally averaged suspended sediment concentration (fourth row) and the suspended sediment transport (bottom row). Note the different scaling of the y-axis at spring and neap tide.

curvature-induced circulation. The top of the right column in Figure 6 is about 1 h after maximum ebb (t = 569.73 d), featuring flow patterns that are largely similar to those 2 h earlier.

[33] At low water slack (t = 569.83 d), the total transports in all three channels were approximately zero. In the top half and bottom half of the water column, the flow was oppositely directed. In the upper layer, flow was mainly from the northern toward the eastern channel, while near the bottom, water flowed from the western and eastern channels into the northern channel. At t = 569.93 d, flow directions had reversed and flood flows occurred in the entire domain of the junction. The bottom of the right column of Figure 6 depicts flow velocities after maximum flood (t = 570.03 d). In the western channel, a clear secondary circulation can be observed, oriented in accordance with curvature.

4.4. Total Water and Freshwater Transports

[34] The middle row of Figure 4 shows that width-integrated transports in the upper and lower layers were different in magnitude and sometimes had opposing directions. At spring tide, the total water transport in the lower layer lagged up to 1 h behind this transport in the upper layers in the northern and western channels (middle of left column in Figure 4). This is in contrast with what is generally observed in homogeneous bottom boundary layer flows, where upper layer flows lag behind lower layer flows due to inertia effects. The eastern channel does show this general characteristic. The phase differences between the upper and lower layers imply that the upper and lower layers have a different exchange pattern. The phase differences between the channels were larger in the lower layers than in the upper layers.

[35] The middle of the right column of Figure 4 shows large differences in the temporal variation of total water transport in the upper and lower layers at neap tide. Especially in the eastern and western channels, transport occurred mainly in the upper layers, while the lower layer was almost stagnant. During ebb tide, transport is predominantly from the northern to the eastern channel. During full flood tide, the transport in the three channels was of equal magnitude. The stronger flood flow in the lower layer of the northern channel than in the upper lower indicates that a pronounced gravitational circulation occurred in this channel.

[36] The freshwater transports (equation (4)) in the upper and lower layers are depicted in the bottom row of Figure 4, which may relate to stratification and the established flow phase differences between the channels. During spring tide, the top to bottom differences in salinity were not very strong. Hence, the transport patterns of freshwater resemble those of total water, albeit that magnitudes were much smaller because of the relatively high salinity. During neap tide, the freshwater transports are nearly proportional to the total water transports, despite the high degree of stratification. This proportionality was caused by the stagnant lower layers of the eastern and the western channels and the relative weak stratification in the northern channel.

4.5. Suspended Sediment Transport

[37] The distribution of the suspended sediment concentration in the cross-sections of the three channels and the flow velocities across the channel are shown in Figure 8 for spring tide. Both the eastern and the western channels are curved. The cross-sectionally averaged currents are not bidirectional. Since fixed along-channel and cross-channel axes were chosen, the cross-sectionally averaged transverse velocities are not necessarily zero. Pronounced secondary flows occurred during high water slack (top row of Figure 7), during high ebb flow velocities (middle row) and during full flood flow (bottom row). In the western channel, the top to bottom difference in flow across the channel was up to 0.6 m s^{-1}. The secondary flow was large with respect to the axial flow velocity magnitude, which was about 0.8 m s^{-1} when the former peaked. The patterns reveal that for most of the period, the flow was toward the inner bend near the bottom and near zero or toward the outer bend near the surface. On the contrary, in the eastern channel, across-channel flow is toward the inner bend near the surface and toward the outer bend near the surface for most of the time. The shallow northern channel also showed strong cross-channel flows, but the patterns were not very clear and are probably related to advected momentum from the other channels.

[38] Figure 7 also shows the observed suspended sediment concentrations. During slack water (top row) the sediment concentrations were larger toward the bottom, but remained below 0.15 kg m^{-3}. At full ebb (middle row) the sediment concentrations were much larger, which may be attributed to local resuspension of sediment from the bed. The secondary flows have likely affected the cross-channel distribution of suspended sediment. In the western channel, suspended sediment was concentrated near the inner bend, where the near-bed cross-channel flow converges. During full flood (bottom row), suspended sediment concentrations were again relatively large at the inner bend of the western channel. This pattern cannot be explained by cross-channel variation in along-channel velocity, which was relatively uniform at that moment. The strong cross-channel flows probably advected the sediment toward the inner bend. Similar conclusions can be drawn from the lowest right panel in Figure 7. It shows a remarkable suspended sediment pattern in the eastern channel during full flood (t = 560.71 d). In the middle of the channel, the suspended sediment concentration peaked at the convergence zone of two relatively weak secondary circulation cells. Such a finger of elevated suspended sediment concentration was observed repeatedly in this channel (results not shown).

[39] The suspended sediment concentrations were multiplied with the along-channel flow velocities and subsequently integrated over the cross-section to obtain the sediment transport. The results for spring tide are shown in the bottom of the left column in Figure 4. The sediment transport shows a different temporal behavior than the freshwater and total water transports. The largest part of the sediment transport takes place in the lower half of the water column. Furthermore, peak sediment transports lag a few hours behind the total and freshwater transport and occur simultaneous in all three channels. In summary, during spring tide, sediment concentrations peaked near the bottom, and the cross-channel distribution was both influenced by local resuspension and by advective processes due to cross-channel flows.

[40] During neap tide, the cross-channel flows were again quite strong, but the flows were not clearly organized in circulation cells (Figure 9). The strongest cross-channel flows were observed in the western and eastern channel near full ebb (top row of Figure 8). Flows across the western channel near the bottom were directed to the outer bend, while near the surface the direction is variable. Due to the stratified water column, flows in the upper and lower parts of the water column were decoupled. Near low water slack (middle row) again the strongest cross-channel flows were present in the western channel. In the middle of this channel, a clear circulation occurred with flows directed to the inner bend near the bottom and toward the outer bend near the surface. This is in agreement with expectations based on channel curvature, but it occurred around slack water and the pattern is not apparent in all parts of the cross-section. During flood flow (bottom row), the cross-channel velocities did not show clear patterns.

[41] The patterns of suspended sediment concentration observed during neap tide (Figure 8) were completely different from observations at spring tide. At neaps, the suspended sediment was confined in the upper 1–2 m of the water column, and the sediment concentrations were a factor 5 to 10 smaller compared to spring tide. The OBS observations showed a gradual decrease going downward in the upper layer, then decreased rapidly around the highest salinity gradient, and remained small up to the bed. The ADCP-derived suspended sediment concentrations were also small in the lowest 50–80% of the water column. During the entire observation period, the suspended matter remained concentrated in the top 1–2 m of the water column. Hence,

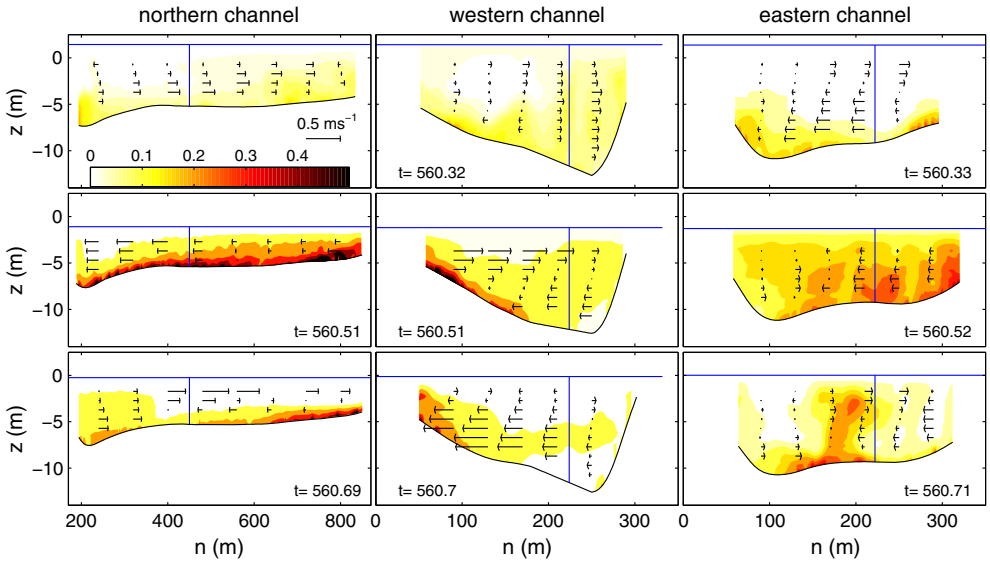

Figure 8. Suspended sediment concentration contours and flow velocity across the channels during three transects at spring tide (facing landward). The moments correspond approximately with the first, third, and fifth moment shown in Figure 5. The vertical blue line indicates the location of the OBS cast.

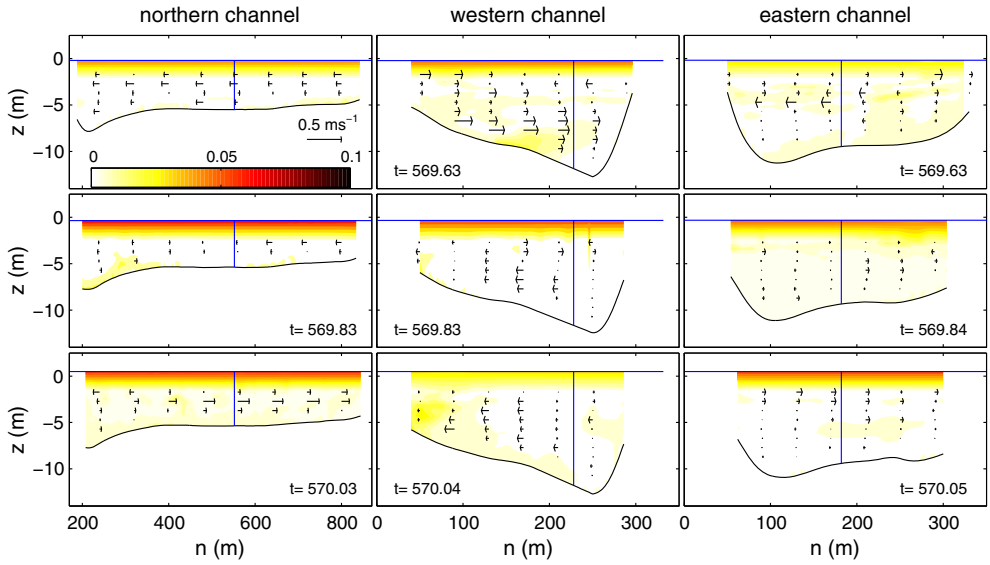

Figure 9. The same as Figure 7, but for three transects during neap tide. The transects correspond with the second, fourth, and sixth moment shown in Figure 6. Note the different color scale with respect to Figure 7.

suspended sediment is mainly transported in the top 2 m of the water column during neap tide. The bottom of the right column in Figure 4 also shows that all sediment transport occurred in the upper layer.

[42] An explanation for the confinement of suspended sediment to the upper layer may be that small-scale plumes [*O'Donnell*, 1993] have been generated during the highly stratified conditions around neap tide. Plume conditions imply that the turbulence in the upper layer is dominated by the turbulence generated in the interior of the fluid rather than by bottom-generated turbulence. In combination with the fine suspended sediment grain sizes corresponding to low fall velocities, the sediment particles remain entrained in the upper layer. Possibly, the small-scale plumes may be generated in the northern channel, where width-averaged depths increase from 3 to 5 m. This would explain why high turbidity in the upper layer was not observed at the junction where the Berau River first splits. Another possibility is that the jump in increasing cross-sectional area from the northern to the combination of the southern and eastern channel resulted in plume formation within the estuary during neap tide.

Table 2. Stokes Transports

Q_S (m^3 s^{-1})	Northern	Western	Eastern
Spring tide	–157	–106	+5
Neap tide	–25	–8	–7

5. Discussion

[43] Based on the results of the two 13 h campaigns, we present four key aspects that determine the intratidal division of water, salt, and suspended sediment at a tidal junction: (1) phase differences in axial flow velocity variations between the channels that join at the tidal junction, (2) effect of secondary flows, (3) baroclinic effects, and (4) role of channel morphology. We compare these four key aspects with general theory on single channel estuaries.

5.1. Phase Differences in Axial Flow Velocity Variation

[44] The cross-sectionally averaged flow velocity showed differences up to 1.5 h between slack water in the three channels connected to the junction (Figure 2). This is mainly caused by differences in geometry and bed roughness between the branches. Although friction differences are unknown, we believe that their role is small with respect to the role of length, depth, and width differences. Apart from details of the tidal propagation, the timing of slack water is also affected by subtidal flows. Subtidal flows are governed by river discharge and by mass transports that compensate for Stokes transport [*Buschman et al.*, 2010; *Sassi et al.*, 2011]. Because the subtidal flow velocity is small with respect to the tidal flow velocity amplitude in each of the channels, the differences in timing of slack waters are dominantly caused by differences in tidal propagation along alternative pathways from the sea to the junction.

[45] The phase differences in tidal flow velocity impact the subtidal transport of water, sediment, and salt. Because water levels in the three channels around the junction are approximately equal, the phase differences imply that the Stokes transports per unit width are different. In a similar way, phase differences in tidal flow will impact the salt transport via the covariation of salinity and flow velocity. Here, we elaborate further on the Stokes transport, but a similar analysis can also be applied to the salt transport. Assuming a constant channel width (W) over time, the Stokes transport (Q_S) in a channel is

$$Q_S = W\langle U'\zeta\rangle, \tag{6}$$

where U' is the variation of the cross-sectionally averaged flow velocity around the tidal average, ζ is the water level variation around the mean level, and angular brackets indicate an average over a tidal cycle. For a progressive wave, the Stokes transport is oriented in the direction of wave propagation. For standing waves, the Stokes transport is zero.

[46] Although we cannot exactly discriminate between the true tidal mean value and the diurnal signal in the data, the fact that the semidiurnal amplitudes of velocity and water level are much larger than the corresponding tidal means and the diurnal variability implies that the Stokes transport can still be determined accurately. We fitted a function composed of a mean, a semi-diurnal, and a quarterdiurnal overtide constituent to the observations. Using the fitted function, we derived the Stokes transport in each channel. The results are shown in Table 2. The absolute values were largest in the northern and western channels. *Buschman et al.* [2010] showed that the sum of the Stokes transports in the channels that connect at a tidal junction are compensated for by return discharges, but that in the individual channels, the Stokes transport is in general not balanced by the return discharge. During neap tide, Stokes transports were small and had a negligible effect on the division of water. During spring tide, however, the effect of the Stokes transport on the discharge distribution was substantial. Because the Stokes transport in the eastern channel was near-zero, it received a larger share of the residual discharge.

5.2. Secondary Flows

[47] Secondary flows clearly impacted the sediment and water division at the junction we studied. Several mechanisms can generate secondary flow [*Lacy and Monismith*, 2001], including centrifugal, advective and Coriolis accelerations, and cross-channel pressure gradients. The forcing is balanced by friction and possibly cross-channel baroclinic pressure gradients [*Chant*, 2002; *Huijts et al.*, 2009]. From our observations we determined the strength of the centrifugal forcing (CF) as

$$CF = \frac{u_{\mathrm{top}}^2 - u_{\mathrm{bot}}^2}{R}, \tag{7}$$

where u_{top} and u_{bot} are the along-channel flow velocity in the bottom half and top half of the cross-section, respectively, and R is the radius of curvature of the bend. The radius of curvature is 400 m for the western and 700 m for the eastern channel.

[48] Figure 10 shows that in the western channel, the strength of the secondary circulation is linearly related to the centrifugal forcing. Interestingly, the constant of variation for ebb flow is clearly larger than during flood. Stratification can enhance cross-channel flows due to reduced friction [*Geyer*, 1993]. However, the water column is more stratified during the flood phase, and one would expect stronger cross-channel flows during flood. Because Coriolis accelerations can be neglected in this area, only advective accelerations or cross-channel pressure gradients can explain the difference between ebb and flood. Based on our observations, we expect that the advective accelerations are of the same order as the centrifugal forcing, confirming the scaling analysis of *Huijts et al.* [2009].

[49] In stratified bends, the secondary flows may develop lateral baroclinic pressure gradients that oppose the helical flow [*Chant*, 2002; *Nidzieko et al.*, 2009]. From a scaling of the cross-channel momentum balance, *Seim and Gregg* [1997] showed that below a threshold of the axial flow velocity, stratification should suppress secondary circulation. Shutting down the secondary circulation would be required for the top to bottom density difference $\Delta\rho = 2.55$ kg m^{-3} for the western channel during spring tide. During neap tide, this critical value is a factor 2–3 smaller. Below these critical values, cross-channel flows can exist. Observations showed that during neap tide, the stratification is very large and indeed no cross-channel flows were

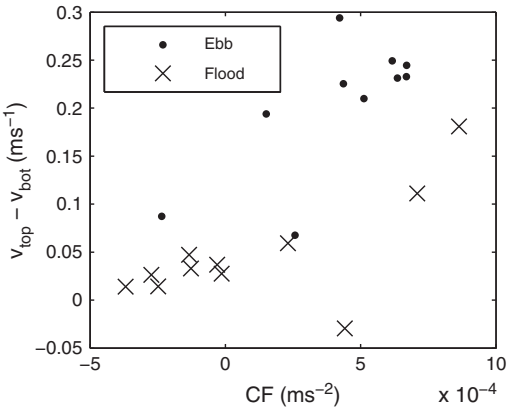

Figure 10. The strength of the secondary circulation as a function of the centrifugal forcing for the western channel during spring tide.

observed. During spring tide, however, we observed strong cross-channel flows, although the stratification was above the critical value.

5.3. Baroclinic Effects

[50] Reversed horizontal density gradients were incidentally observed (top row of Figure 4), meaning that salinity decreased going seaward. Although such a salinity distribution may be commonly observed in inversed estuaries [*Wolanski*, 1986], it has rarely been observed in estuaries with a substantial fresh water input. The reversal of the density gradients can be related to the asymmetry of the delta channel network.

[51] Differences in length and width between the channels that connect at the junction probably affect the transport of salinity in the system in two ways. First, the phase differences in flow variation between the channels may result in regions of a reversed salinity gradient. This happens especially around slack water. Second, since salinity at sea and at the junction is for both sea-connected channels the same, their length differences result in a different along-channel salinity gradient. This influences the regional stratification dynamics. Due to exchange of water and salt between channels and phase differences in axial flow variation, the stratification dynamics in a channel close to a tidal junction is more complex than in a single estuarine channel.

[52] The levels of the potential energy anomaly ϕ (middle row of Figure 4) were exceptionally large during neap tide, nearly reaching 200 J m^{-3}. These levels are well over maximum values reported in recent studies focusing on tidal embayments [*Howlett et al.*, 2011; *Hoitink et al.*, 2011], a shallow sound [*Hofmeister et al.*, 2009], and an idealized estuary [*Burchard and Hofmeister*, 2008]. The bottom row in Figure 4 shows rates of change of ϕ by mixing, which are not particularly low during spring tide. The anomalously high absolute values of ϕ can be attributed to differential advection of salinity by converging flows at the junction. Flows with a highly different origin converge at the junction, creating high levels of stratification. Strong stratification may suppress secondary circulation, which in turn may impact on the division of water and sediment at the junction.

5.4. Implications for Morphology

[53] The flow divergence and convergence at a tidal junction have implications for the morphology of the channels around the tidal junction. At river bifurcations, a small or shallow channel on the seaside is likely to silt up eventually [*Kleinhans et al.*, 2008]. At a tidal junction, sediment may be deposited during low flow conditions. Around spring tide, however, periods with high axial flow velocity magnitudes occur. Due to the flow variation and its phase differences between the channels, periods with high axial flow velocity magnitude occur in each of the channels. During these periods, the earlier deposited sediment is resuspended and transported away from the tidal junction. Moreover, secondary flow patterns and suspended sediment redistribution vary during a tidal cycle, which may also enhance resuspension from the bed in the channels around the tidal junction.

[54] Based on a study on experimental river bifurcations, *Thomas et al.* [2011] reasoned that the channels downstream of an asymmetric bifurcation may remain open due to the enhanced secondary circulation in these channels. Averaged over a spring-neap tidal cycle, the periodically elevated sediment transport capacity in each of the channels may imply that all three channels remain open. The effect of the phase differences in flow variation on the bathymetry is illustrated by trenches at the tidal junction, including a trench in between the sea-connected eastern and western branches (bottom of Figure 1). Also the bathymetry of the entire tidal network [*Buschman*, 2011] shows that channels close to tidal junctions are generally deeper than the single channels further away from the junctions.

6. Conclusions

[55] Flow velocity, salinity, and suspended sediment concentration were observed in the three channels around a stratified tidal junction in an Indonesian tidal network. Observations were carried out during a tidal cycle at spring tide and at neap tide.

[56] At spring tide, peak flow velocities around the junction could exceed 1 m s^{-1}, the major source of sediment was resuspension, and the water column was partially stratified. We observed phase differences in flow velocity variation

between the three channels of up to 2 h. These phase differences strongly influenced the exchange of water, salt, and sediment at the junction.

[57] At neap tide, we observed a salt wedge salinity structure with very high potential energy anomaly. The suspended sediment was concentrated in the thin fresh water layer near the surface. Along-channel flows in the upper and lower layers strongly differed in magnitude and sometimes even in direction. The lower layer in the eastern and western channels was often stagnant. The division of water, sediment, and salt occurred predominantly in the upper layers.

[58] Based on these observations, transport of water, salt, and sediment in channels around a tidal junction is compared to these transports in single channel estuaries.

[59] 1. Although the water level variation is similar in the channels close to a tidal junction as in single channel estuaries, phase differences in the axial flow variations between the three channels may be considerable. These phase differences cause that the Stokes transports are different, which generally results in a net circulation in the tidal network [*Buschman et al.*, 2010].

[60] 2. The exchange of water and salt between the three channels, in combination with the flow phase differences, may locally result in higher along-channel salinity gradients than observed in single channel estuaries. The differences in tidal propagation related to the geometry of the channels seaward of a junction partly determine the salinity differences at the junctions. Occasionally, salinity may increase in the landward direction. In turn, the along-channel and cross-channel baroclinic pressure gradients affect the exchanges.

[61] 3. A tidal junction implies that at least one of the channels around the junction is curved. At the junction under study, two of the three channels were sharply curved. The secondary circulation in one of these channels was most pronounced during spring tide. In general, freshwater is dominantly transported in the upper layer and sediment in the lower layer. Hence, secondary circulation in channels around a tidal junction affects the division of freshwater and sediment over the receiving channels.

[62] 4. Bed level gradients in the surroundings of a tidal junction may be larger than in single channel estuaries, since the periodically elevated sediment transport capacity in each of the channels enhances erosion.

[63] **Acknowledgments.** This study was supported by grant WT 77-203 of WOTRO Science for Global Development, a division of the Netherlands Organisation of Scientific Research (NWO). M.C.G. van Maarseveen (Utrecht University) is acknowledged for preparing and maintaining the instruments and his technical assistance. We thank A. Tarya and E. Wielsma (Utrecht University) for their assistance in the field campaigns. Eric de Lande performed the first analysis of data at this tidal junction. We are grateful for the comments by M.G. Sassi (Wageningen University) and H.E. de Swart (Utrecht University) on an earlier version of this manuscript. Two reviewers are acknowledged for their comments and suggestions to improve this paper.

References

Burchard, H., and R. Hofmeister (2008), A dynamic equation for the potential energy anomaly for analysing mixing and stratification in estuaries and coastal seas, *Estuarine Coastal Shelf Sci.*, *77*(4), 679–687, doi:10.1016/j.ecss.2007.10.025.

Buschman, F. A. (2011), Flow and sediment transport in an Indonesian tidal network, PhD thesis, Utrecht Studies in Earth Sciences, Utrecht.

Buschman, F. A., A. J. F. Hoitink, M. van der Vegt, and P. Hoekstra (2009), Subtidal water level variation controlled by river flow and tides, *Water Resour. Res.*, *45*(W10420), 1–12, doi:10.1029/2009WR008167.

Buschman, F. A., A. J. F. Hoitink, M. van der Vegt, and P. Hoekstra (2010), Subtidal flow division at a shallow tidal junction, *Water Resour. Res.*, *46*(W12515), doi:10.1029/2010WR009266.

Buschman, F. A., S. M. de Jong, and P. Hoekstra (2011), Hoitink, A. J. F., *Hydrol. Earth Syst. Sc. Discuss*, *8*, 7137–7175, doi:10.5194/hessd-8-7137-2011.

Chant, R. J. (2002), Secondary circulation in a region of flow curvature: Relationship with tidal forcing and river discharge, *J. Geophys. Res.*, *107*(C9), doi:10.1029/2001JC001082.

Deines, K. L. (1999), Backscatter estimation using broadband acoustic Doppler current profilers, In *Proceedings of the IEEE Sixth Working Conference on Current Measurement*, vol. 99, pp. 249–253, San Diego, USA, doi:10.1109/CCM.1999.755249.

Downing, A., P. D. Thorne, and C. Vincent (1995), Backscattering from a suspension in the near-field of a piston transducer, *J. Acoust. Soc. Am.*, *97*(3), 1614–1620.

Dyer, K. R. (1986), *Coastal and Estuarine Sediment Dynamics*, Wiley, Chichester.

Fassnacht, S. R. (1997), A multi-channel suspended sediment transport model for the Mackenzie delta, Northwest territories, *J. Hydrol.*, *197*, 128–145.

Fassnacht, S. R. (2000), Flow modelling to estimate suspended sediment travel times for two Canadian deltas, *Hydrol. Earth Syst. Sc.*, *4*(3), 425–438.

Gartner, J. W. (2004), Estimating suspended solids concentrations from backscatter intensity measured by acoustic Doppler current profiler in San Francisco Bay, California, *Mar. Geol.*, *211*, 169–187, doi:10.1016/j.margeo.2004.07.001.

Geyer, W. R. (1993), Three-dimensional tidal flow around headlands, *J. Geophys. Res.*, *98*(C1), 955–966.

Hofmeister, R., H. Burchard, and K. Bolding (2009), A three-dimensional model study on processes of stratification and de-stratification in the Limfjord, *Cont. Shelf Res.*, *29*(11-12), 1515–1524, doi:10.1016/j.csr.2009.04.004.

Hoitink, A. J. F., and P. Hoekstra (2005), Observations of suspended sediment from ADCP and OBS measurements in a mud-dominated environment, *Coastal Eng.*, *52*, 103–118, doi:10.1016/j.coastaleng.2004.09.005.

Hoitink, A. J. F., D. S. van Maren, and P. Hoekstra (2011), Mixing and stratification in a tropical tidal embayment subject to a distributed freshwater source, *J. Mar. Sys.*, *88*(1), 34–44, doi:10.1016/j.jmarsys.2011.02.015.

Howlett, E. R., T. P. Rippeth, and J. Howarth (2011), Processes contributing to the evolution and destruction of stratification in the Liverpool Bay ROFI, *Ocean Dyn.*, *61*(9), 1403–1419, doi:10.1007/s10236-011-0402-y.

Huijts, K. M. H., H. M. Schuttelaars, H. E. de Swart, and A. Valle-Levinson (2006), Lateral entrapment of sediment in tidal estuaries: An idealized model study, *J. Geophys. Res.*, *111*(C12), doi:10.1029/2006JC003615.

Huijts, K. M. H., H. M. Schuttelaars, H. E. de Swart, and C. T. Friedrichs (2009), Analytical study of the transverse distribution of along-channel and transverse residual flows in tidal estuaries, *Cont. Shelf Res.*, *29*, 89–100, doi:10.1016/j.csr.2007.09.007.

Jay, D. A., and E. P. Flinchem (1990), Circulation, density distribution and neap-spring transitions in the Columbia River Estuary, *Prog. Oceanogr.*, *25*(1–4), 81–112, doi:10.1016/0079-6611(90)90004-L.

Kim, Y. H., and G. Voulgaris (2005), Effect of channel bifurcation on residual estuarine circulation: Winyah Bay, South Carolina, *Estuarine Coastal Shelf Sci.*, *65*, 671–686.

Kleinhans, M. G., H. R. A. Jagers, E. Mosselman, and C. Sloff (2008), Bifurcation dynamics and avulsion duration in meandering rivers by one-dimensional and three-dimensional models, *Water Resour. Res.*, *44*(W08454), 1–31.

Kleinhans, M. G., R. I. Ferguson, S. N. Lane, and R. J. Hardy (2013), Splitting rivers at their seams: Bifurcations and avulsions, *Earth Surf. Proc. Land.*, *38*(1), 47–61, doi:10.1002/esp.3268.

Lacy, J. R., and S. G. Monismith (2001), Secondary currents in a curved, stratified, estuarine channel, *J. Geophys. Res.*, *106*(C12), 31,283–31,302, doi:10.1029/2000JC000606.

Lerczak, J. A., and W. R. Geyer (2004), Modeling the lateral circulation in straight, stratified estuaries, *J. Phys. Oceanogr.*, *34*(6), 1410–1428, doi:10.1175/1520-0485(2004)034<1410:MTLCIS>2.0.CO;2.

Muste, M., K. Yu, and M. Spasojevic (2004), Practical aspects of ADCP data use for quantification of mean river flow characteristics; part 1: Moving-vessel measurements, *Flow Meas. Instrum.*, *15*, doi:10.1016/j.flowmeasinst.2003.09.001.

Nidzieko, N. J., J. L. Hench, and S. G. Monismith (2009), Lateral circulation in well-mixed and stratified estuarine flows with curvature, *J. Phys. Oceanogr.*, *39*(4), 831–851, doi:10.1175/2008JPO4017.1.

O'Donnell, J. (1993), Surface fronts in estuaries: A review, *Estuaries*, *16*(1), 12–39

Prandle, D. (2004), How tides and river flows determine estuarine bathymetries, *Prog. Oceanogr.*, *61*, 1–26

Sassi, M. G., A. J. F. Hoitink, B. de Brye, B. Vermeulen, and E. Deleersnijder (2011), Tidal impact on the division of river discharge over distributary channels in the Mahakam Delta, *Ocean Dyn.*, *61*, 1–18, doi: 10.1007/s10236-011-0473-9.

Seim, H., J. Blanton, and S. Elston (2006), Tidal circulation and energy dissipation in a shallow sinuous estuary, *Ocean Dyn.*, *56*(3–4), 360–375, doi:10.1007/s10236-006-0078-X.

Seim, H. E., and M. C. Gregg (1997), The importance of aspiration and channel curvature in producing strong vertical mixing over a sill, *J. Geophys. Res.*, *102*(C2), 3451–3472.

Simpson, J. H. (1981), The shelf-sea fronts: Implications of their existence and behaviour, *Proc. R. Soc. (London) A*, *302*, 531–546.

Stacey, M. T., J. R. Burau, and S. G. Monismith (2001), Creation of residual flows in a partially stratified estuary, *J. Geophys. Res.*, *106*(C8), 17,013–17,037

Tarya, A., A. J. F. Hoitink, and M. van der Vegt (2010), Tidal and subtidal flow patterns on a tropical continental shelf semi-insulated by coral reefs, *J. Geophys. Res.*, *115*(C09029), doi:10.1029/2010JC006168.

Thomas, R. E., D. R. Parsons, S. D. Sandbach, G. M. Keevil, W. A. Marra, R. J. Hardy, J. L. Best, S. N. Lane, and J. A. Ross (2011), An experimental study of discharge partitioning and flow structure at symmetrical bifurcations, *Earth Surf. Proc. Land.*, *36*, 2069–2082, doi: 10.1002/esp.2231.

Thorne, P. D., and D. M. Hanes (2002), A review of acoustic measurement of small-scale sediment processes, *Cont. Shelf Res.*, *22*, 603–632

Turner, A., and G. E. Millward (2002), Suspended particles: Their role in estuarine biogeochemical cycles, *Estuarine Coastal Shelf Sci.*, *55*, 857–883, doi:10.1006/ecss.2002.1033.

Warner, J., D. Schoellhamer, J. Burau, and G. Schladow (2002), Effects of tidal current phase at the junction of two straits, *Cont. Shelf Res.*, *22* (11–13), 1629–1642.

Warner, J. C., D. Schoellhamer, and G. Schladow (2003), Tidal truncation and barotropic convergence in a channel network tidally driven from opposing entrances, *Estuarine Coastal Shelf Sci.*, *56*, 629–639, doi: 10.1016/S0272-7714(02)00213-5.

Wolanski, E. (1986), An evaporation-driven salinity maximum zone in Australian tropical estuaries, *Estuarine Coastal Shelf Sci.*, *22*(4), 415–424, doi:10.1016/0272-7714(86)90065-X.